# Generalized Monte Carlo approach for the study of the coherent ultrafast carrier dynamics in photoexcited semiconductors

Stefan Haas and Fausto Rossi
*Fachbereich Physik und Zentrum für Materialwissenschaften, Philipps-Universität Marburg, Renthof 5, 35032 Marburg, Germany*

Tilmann Kuhn*
*Lehrstuhl für Theoretische Physik, Brandenburgische Technische Universität, Postfach 101344, 03013 Cottbus, Germany*
(Received 2 November 1995)

A generalized Monte Carlo method for the solution of the coupled set of kinetic equations for the distribution functions and the interband polarization is presented. The aim of this method is to combine the advantages of the description within a fully quantum mechanical picture with the power of the Monte Carlo technique for the treatment of stochastic processes. It is based on a decomposition of the kinetic equations in a coherent and an incoherent part. The former is integrated directly while the latter is sampled by means of a Monte Carlo simulation. This allows us to treat on the same kinetic level carrier thermalization and relaxation as well as dephasing processes. In particular, the problem of photogeneration and its theoretical description is discussed. The equations of motion including the relevant scattering contributions are derived and presented in a way that emphasizes the symmetry between distribution functions and polarization. The scattering terms for the polarization are discussed in detail. We show that some of the approaches commonly used fail in describing correctly the effect of carrier-carrier interaction in the low-density limit. By including terms that have the structure of ''in-scattering'' terms for the interband polarization, the experimentally observed features in the carrier dynamics are well described in the whole density range.

## I. INTRODUCTION

The Monte Carlo method, which has been applied for more than 25 years to the analysis of semiclassical transport and relaxation processes in semiconductors,[1–9] has been recognized to be the most powerful numerical tool for microelectronic device simulation based on microscopic scattering rates.[10–12] On the other hand, the present-day technology allows the investigation of relaxation phenomena in semiconductors with a time resolution that has now reached a few femtoseconds.[5,13–17] On such a time scale, coherent aspects play an important role even for experiments that mainly probe the dynamics of carrier distributions.[16,18,19] In this case the carrier dynamics cannot be treated in terms of the traditional semiclassical transport theory where the carrier system is completely specified by the respective distribution functions. Instead, the interband polarization has to be included as an independent variable.[20–23] In order to study this partially coherent dynamics, a generalization of the conventional Monte Carlo method is required.

The aim of the present paper is to present both the theoretical background and the technical aspects of a method recently proposed by the authors[18,23,24] as well as to discuss its application to the analysis of ultrafast carrier dynamics in photoexcited semiconductors.[16,18] The main peculiarity of the proposed approach is to retain the big advantages of the Monte Carlo method in treating scattering processes and, at the same time, to take into account on the same kinetic level also coherent phenomena. Compared to the conventional Monte Carlo technique, which simply provides a solution of the semiclassical Boltzmann transport equation (BTE), this generalized Monte Carlo approach provides a solution of the semiconductor Bloch equations (SBE). In addition to a simulation of the various distribution functions, this will result in a Monte Carlo simulation of the scattering dynamics of the interband polarization induced by the coherent light field.

Such an approach allows a self-consistent description of the carrier photogeneration process.[16,18] The energy broadening due to the finite pulse duration and due to the decay of the interband polarization has not to be introduced as a phenomenological parameter as in any conventional Monte Carlo simulation[5,25] but it comes out self-consistently with its full time dependence. However, in a recent paper[18] we have shown that a dephasing rate approximation (given by the total scattering rate), which is often performed to simplify the dynamics of the polarization,[22,23] completely fails in the case of carrier-carrier scattering at low densities by strongly overestimating the dephasing of the interband polarization. Including additional contributions with the structure of ''in-scattering terms'' in the equations of motion of the polarization, on the other hand, resulted in a physically reasonable density dependence of the carrier dynamics. Using this model, a very good agreement between calculated and measured band-to-acceptor luminescence spectra in $p$-doped GaAs has been found that demonstrates the importance of a correct treatment of the dynamics of the interband polarization.[16]

The strong symmetry between the equations of motion for the distribution functions and for the polarization motivates the use of a Monte Carlo technique also for the solution of the latter equation. The main objective of this paper is to discuss in detail this extension of the conventional Monte Carlo method to the simulation of a complex quantity, e.g., the interband polarization, and to present new results where we particularly emphasize the scattering dynamics of the interband polarization; this allows us to gain insight into the

 

details of the dephasing process, which is the result of the interplay between three different contributions: coherent rotation, in-scattering, and out-scattering terms.

The paper is organized as follows: In Sec. II we derive the equations of motion by extending the density matrix approach given in Ref. 23 to the case of carrier-carrier scattering in a two-band model. The scattering contributions are written in a way that emphasizes the symmetry between distribution functions and polarization. In Sec. III we discuss the numerical approach that has been applied for the solution of the equations of motion. Section IV is devoted to the results of the simulations. In particular, a detailed analysis of the scattering dynamics of the polarization at various densities is given that shows the big reduction of the dephasing at low densities due to cancellation effects. Finally, in Sec. V some conclusions are drawn.

## II. THEORETICAL APPROACH

In this paper we study the carrier dynamics in a direct-gap semiconductor during and after an ultrashort laser excitation. We consider a bulk semiconductor with two isotropic, parabolic bands, the conduction band and the heavy-hole band. The carriers interact via the Coulomb potential. Furthermore they interact with phonons. For reasons of simplicity we discuss only the case of Fröhlich interaction with LO phonons, which is typically the most important carrier-phonon interaction for the ultrafast carrier dynamics.

The system is described by a Hamiltonian that can be decomposed into parts $H_0$ and $H_1$. In $H_0$ we consider those parts that can be treated exactly within a single-particle picture. The remaining contributions that have to be treated within some approximation scheme are considered in $H_1$. For reasons of simplicity we neglect the spin index in the calculations; in the numerical results, however, it has been taken into account.

We describe the dynamics of our physical system in terms of the density-matrix approach. The basic variables for the kinetics of the system are the distribution functions (intraband density matrices) of electrons, holes, and phonons,

$$f_{\mathbf{k}}^{e}=\langle c_{\mathbf{k}}^{\dagger}c_{\mathbf{k}}\rangle, \quad f_{\mathbf{k}}^{h}=\langle d_{\mathbf{k}}^{\dagger}d_{\mathbf{k}}\rangle, \quad \text{and} \quad n_{\mathbf{q}}=\langle b_{\mathbf{q}}^{\dagger}b_{\mathbf{q}}\rangle, \tag{1}$$

with $c_{\mathbf{k}}^{\dagger}, d_{\mathbf{k}}^{\dagger}, b_{\mathbf{q}}^{\dagger}$ ($c_{\mathbf{k}}, d_{\mathbf{k}}, b_{\mathbf{q}}$) denoting creation (annihilation) operators of electrons, holes, phonons, respectively. To take into account the coherence induced by the external laser field, we have to consider explicitly the interband polarization (interband density matrix)

$$p_{\mathbf{k}}=\langle d_{-\mathbf{k}}c_{\mathbf{k}}\rangle \quad \text{and} \quad p_{\mathbf{k}}^{*}=\langle c_{\mathbf{k}}^{\dagger}d_{-\mathbf{k}}^{\dagger}\rangle. \tag{2}$$

### A. Single-particle Hamiltonian

The single-particle Hamiltonian describing the free carriers interacting with a classical light field as well as the free phonons is given by[26]

$$H_0=\sum_{\mathbf{k}}\epsilon_{\mathbf{k}}^{e}c_{\mathbf{k}}^{\dagger}c_{\mathbf{k}}+\sum_{\mathbf{k}}\epsilon_{\mathbf{k}}^{h}d_{\mathbf{k}}^{\dagger}d_{\mathbf{k}}+\sum_{\mathbf{q}}\hbar\omega_{\mathbf{q}}b_{\mathbf{q}}^{\dagger}b_{\mathbf{q}} + \sum_{\mathbf{k}}\left[M_{\mathbf{k}}E_0(t)e^{-i\omega_L t}c_{\mathbf{k}}^{\dagger}d_{-\mathbf{k}}^{\dagger}+M_{\mathbf{k}}^{*}E_0^{*}(t)e^{i\omega_L t}d_{-\mathbf{k}}c_{\mathbf{k}}\right], \tag{3}$$

where $\epsilon_{\mathbf{k}}^{e}=E_g+\hbar^2k^2/(2m_e)$ and $\epsilon_{\mathbf{k}}^{h}=\hbar^2k^2/(2m_h)$ denote the energies of electron and hole states, $m_e$ and $m_h$ the respective effective masses, $E_g$ the band gap, $\omega_{\mathbf{q}}$ the dispersion relation of the phonons, $M_{\mathbf{k}}$ the dipole matrix element, and $E_0(t)$ the amplitude of the external light field with frequency $\omega_L$. The interaction is treated in dipole and rotating-wave approximation and we do not include any polarization effects of the laser light.

Using the Heisenberg equations of motion one obtains

$$\left.\frac{d}{dt}f_{\mathbf{k}}^{e}\right|^{(0)}=\left.\frac{d}{dt}f_{-\mathbf{k}}^{h}\right|^{(0)}=g_{\mathbf{k}}^{(0)}(t), \tag{4}$$

$$\left.\frac{d}{dt}p_{\mathbf{k}}\right|^{(0)}=\frac{1}{i\hbar}\left[(\epsilon_{\mathbf{k}}^{e}+\epsilon_{-\mathbf{k}}^{h})p_{\mathbf{k}}+M_{\mathbf{k}}E_0(t)e^{-i\omega_L t}(1-f_{\mathbf{k}}^{e}-f_{-\mathbf{k}}^{h})\right] \tag{5}$$

with the generation rate

$$g_{\mathbf{k}}^{(0)}(t)=\frac{1}{i\hbar}\left[M_{\mathbf{k}}E_0(t)e^{-i\omega_L t}p_{\mathbf{k}}^{*}-M_{\mathbf{k}}^{*}E_0^{*}(t)e^{i\omega_L t}p_{\mathbf{k}}\right]. \tag{6}$$

This system of equations describes an ensemble of two-level systems coherently driven by the external light field. The semiclassical generation rate is obtained by an adiabatic elimination of the polarization as discussed in Ref. 23.

### B. Carrier-phonon interaction

In the absence of an external light field the electron states are eigenstates of an ideal periodic lattice. Deviations from this idealized periodicity due to lattice vibrations lead to a coupling of the different electron states. This interaction is described by the carrier-phonon (cp) Hamiltonian:[26,27]

$$H_1^{\mathrm{cp}}=\sum_{\mathbf{q},\mathbf{k}}\left[\gamma_{\mathbf{q}}^{e}c_{\mathbf{k}+\mathbf{q}}^{\dagger}b_{\mathbf{q}}c_{\mathbf{k}}+\gamma_{\mathbf{q}}^{e*}c_{\mathbf{k}}^{\dagger}b_{\mathbf{q}}^{\dagger}c_{\mathbf{k}+\mathbf{q}}+\gamma_{\mathbf{q}}^{h}d_{\mathbf{k}+\mathbf{q}}^{\dagger}b_{\mathbf{q}}d_{\mathbf{k}} + \gamma_{\mathbf{q}}^{h*}d_{\mathbf{k}}^{\dagger}b_{\mathbf{q}}^{\dagger}d_{\mathbf{k}+\mathbf{q}}\right]. \tag{7}$$

Here, $\gamma_{\mathbf{q}}^{e,h}$ are the coupling matrix elements for polar or deformation-potential interaction for electrons or holes. In the case of a polar interaction, due to the opposite charge of electrons and holes, the coupling constants are related by $\gamma_{\mathbf{q}}^{e}=-\gamma_{\mathbf{q}}^{h}=\gamma_{\mathbf{q}}$.

Starting from this Hamiltonian, the cp contribution to the equation of motion, e.g., of the electron distribution function, is given by

$$\left.\frac{d}{dt}f_{\mathbf{k}}^{e}\right|^{\mathrm{cp}}=\frac{1}{i\hbar}\sum_{\mathbf{q}}\left\{\gamma_{\mathbf{q}}\left[\langle c_{\mathbf{k}}^{\dagger}b_{\mathbf{q}}c_{\mathbf{k}-\mathbf{q}}\rangle-\langle c_{\mathbf{k}+\mathbf{q}}^{\dagger}b_{\mathbf{q}}c_{\mathbf{k}}\rangle\right] + \gamma_{\mathbf{q}}^{*}\left[\langle c_{\mathbf{k}}^{\dagger}b_{\mathbf{q}}^{\dagger}c_{\mathbf{k}+\mathbf{q}}\rangle-\langle c_{\mathbf{k}-\mathbf{q}}^{\dagger}b_{\mathbf{q}}^{\dagger}c_{\mathbf{k}}\rangle\right]\right\} \tag{8}$$

involving phonon-assisted density matrices.[28] The derivation of the contributions up to second order in the coupling matrix element in the Markov approximation is discussed in detail in Ref. 23. There, however, terms involving simultaneously electron-phonon and hole-phonon interaction have been neglected, which resulted in a dephasing rate $\Gamma_{\mathbf{k}}$. If they are included, the total second-order cp contributions to the equations of motion of distribution functions and polarization are given by

$$\left.\frac{d}{dt}f^e_{\mathbf{k}}\right|^{(\mathrm{cp},2)} = -\sum_{\mathbf{q}} \left[W^{e(\mathrm{cp})}_{\mathbf{k}-\mathbf{q},\mathbf{k}} f^e_{\mathbf{k}} - W^{e(\mathrm{cp})}_{\mathbf{k},\mathbf{k}-\mathbf{q}} f^e_{\mathbf{k}-\mathbf{q}}\right] + \frac{1}{i\hbar}\left[\Delta^{e(\mathrm{cp})}_{\mathbf{k}} p^*_{\mathbf{k}} - \Delta^{e(\mathrm{cp})*}_{\mathbf{k}} p_{\mathbf{k}}\right], \tag{9}$$

$$\left.\frac{d}{dt}f^h_{\mathbf{k}}\right|^{(\mathrm{cp},2)} = -\sum_{\mathbf{q}} \left[W^{h(\mathrm{cp})}_{\mathbf{k}-\mathbf{q},\mathbf{k}} f^h_{\mathbf{k}} - W^{h(\mathrm{cp})}_{\mathbf{k},\mathbf{k}-\mathbf{q}} f^h_{\mathbf{k}-\mathbf{q}}\right] + \frac{1}{i\hbar}\left[\Delta^{h(\mathrm{cp})}_{-\mathbf{k}} p^*_{-\mathbf{k}} - \Delta^{h(\mathrm{cp})*}_{-\mathbf{k}} p_{-\mathbf{k}}\right], \tag{10}$$

$$\left.\frac{d}{dt}p_{\mathbf{k}}\right|^{(\mathrm{cp},2)} = -\sum_{\mathbf{q}} \left[\mathscr{W}^{p(\mathrm{cp})}_{\mathbf{k}-\mathbf{q},\mathbf{k}} p_{\mathbf{k}} - \mathscr{W}^{p(\mathrm{cp})}_{\mathbf{k},\mathbf{k}-\mathbf{q}} p_{\mathbf{k}-\mathbf{q}}\right], \tag{11}$$

with

$$W^{e,h(\mathrm{cp})}_{\mathbf{k}-\mathbf{q},\mathbf{k}} = \frac{2\pi}{\hbar}\sum_{\pm} |\gamma_{\mathbf{q}}|^2 \delta(\epsilon^{e,h}_{\mathbf{k}-\mathbf{q}} - \epsilon^{e,h}_{\mathbf{k}} \pm \hbar\omega_{\mathbf{q}})(n_{\mathbf{q}} + \tfrac{1}{2} \pm \tfrac{1}{2})(1 - f^{e,h}_{\mathbf{k}-\mathbf{q}}), \tag{12}$$

$$\mathscr{W}^{p(\mathrm{cp})}_{\mathbf{k}-\mathbf{q},\mathbf{k}} = \frac{\pi}{\hbar}\sum_{\nu=e,h}\sum_{\pm} |\gamma_{\mathbf{q}}|^2 \{\mathscr{D}(\epsilon^{\nu}_{\mathbf{k}-\mathbf{q}} - \epsilon^{\nu}_{\mathbf{k}} \pm \hbar\omega_{\mathbf{q}})[(n_{\mathbf{q}} + \tfrac{1}{2} \mp \tfrac{1}{2}) f^{\nu}_{\mathbf{k}-\mathbf{q}} + (n_{\mathbf{q}} + \tfrac{1}{2} \pm \tfrac{1}{2})(1 - f^{\nu}_{\mathbf{k}-\mathbf{q}})], \tag{13}$$

$$\Delta^{e,h(\mathrm{cp})}_{\mathbf{k}} = i\pi\sum_{\mathbf{q}} |\gamma_{\mathbf{q}}|^2 \sum_{\pm} (\pm p_{\mathbf{k}-\mathbf{q}}) \mathscr{D}(\epsilon^{h,e}_{\mathbf{k}} - \epsilon^{h,e}_{\mathbf{k}-\mathbf{q}} \pm \hbar\omega_{\mathbf{q}}). \tag{14}$$

Here, the function $\mathscr{D}(\epsilon)$ is defined as

$$\mathscr{D}(\epsilon) = \delta(\epsilon) + \frac{1}{i\pi}\frac{\mathscr{P}}{\epsilon} \tag{15}$$

with $\mathscr{P}$ denoting the principal value. The quantities $\Delta^{e,h(\mathrm{cp})}_{\mathbf{k}}$ appear in the same way as the laser field in the equations of motion for the distribution functions. Therefore, they can be interpreted as internal fields that, however, are different for electrons and holes. In the polarization equation the field is not renormalized. The structure of Eqs. (9)–(11) clearly shows a symmetry between distribution functions and polarization: In both cases we may identify terms with the structure of ''out-scattering'' processes ($\propto f_{\mathbf{k}}, p_{\mathbf{k}}$) and terms with the structure of ''in-scattering'' processes ($\propto f_{\mathbf{k}-\mathbf{q}}, p_{\mathbf{k}-\mathbf{q}}$). The main difference is the fact that, in contrast to the distribution functions, the polarization and the respective matrices in Eq. (11) are complex quantities. We will come back to this point later.

### C. Carrier-carrier interaction

The charged carriers interact via the Coulomb potential $V_{\mathbf{q}}$. We consider in our two-band model only processes conserving the number of particles per band. Thus Auger recombination and impact ionization are neglected. These processes are usually considered to become important at very high densities or at energies high up in the band.

The Hamiltonian describing carrier-carrier (cc) interaction is given by

$$H^{\mathrm{cc}}_1 = \sum_{\mathbf{k},\mathbf{k}',\mathbf{q}} V_{\mathbf{q}}\left[\tfrac{1}{2} c^{\dagger}_{\mathbf{k}} c^{\dagger}_{\mathbf{k}'} c_{\mathbf{k}'+\mathbf{q}} c_{\mathbf{k}-\mathbf{q}} + \tfrac{1}{2} d^{\dagger}_{\mathbf{k}} d^{\dagger}_{\mathbf{k}'} d_{\mathbf{k}'+\mathbf{q}} d_{\mathbf{k}-\mathbf{q}} - c^{\dagger}_{\mathbf{k}} d^{\dagger}_{-\mathbf{k}'} d_{-\mathbf{k}'+\mathbf{q}} c_{\mathbf{k}-\mathbf{q}}\right]. \tag{16}$$

The first two parts are the repulsive electron-electron and hole-hole interaction terms, the third one describes the attractive interaction between electrons and holes. The presence of free carriers leads to a screening of the Coulomb potential. It is not the aim of the present paper to discuss the derivation of the screened potential, instead we simply use a Lindhard-like static screening[26] (see Appendix A).

The cc contribution to the equation of motion, e.g., of the electron distribution function, is given by

$$\left.\frac{d}{dt}f^e_{\mathbf{k}}\right|^{\mathrm{cc}} = \frac{1}{i\hbar}\sum_{\mathbf{k}',\mathbf{q}} V_{\mathbf{q}}\left[\langle c^{\dagger}_{\mathbf{k}} c^{\dagger}_{\mathbf{k}'} c_{\mathbf{k}'+\mathbf{q}'} c_{\mathbf{k}-\mathbf{q}}\rangle - \langle c^{\dagger}_{\mathbf{k}-\mathbf{q}} c^{\dagger}_{\mathbf{k}'+\mathbf{q}} c_{\mathbf{k}'} c_{\mathbf{k}}\rangle - \langle c^{\dagger}_{\mathbf{k}} d^{\dagger}_{-\mathbf{k}'-\mathbf{q}} d_{-\mathbf{k}'} c_{\mathbf{k}-\mathbf{q}}\rangle + \langle c^{\dagger}_{\mathbf{k}-\mathbf{q}} d^{\dagger}_{-\mathbf{k}'} d_{-\mathbf{k}'-\mathbf{q}} c_{\mathbf{k}}\rangle\right] \tag{17}$$

involving two-particle density matrices and leading to an infinite hierarchy of equations of motion.[29] The first-order contributions (Hartree-Fock terms) are obtained by factorization according to

$$\left.\frac{d}{dt}f^e_{\mathbf{k}}\right|^{(\mathrm{cc},1)} = \left.\frac{d}{dt}f^h_{-\mathbf{k}}\right|^{(\mathrm{cc},1)} = \frac{1}{i\hbar}\left[\Delta_{\mathbf{k}} p^*_{\mathbf{k}} - \Delta^*_{\mathbf{k}} p_{\mathbf{k}}\right], \tag{18}$$

$$\left.\frac{d}{dt}p_{\mathbf{k}}\right|^{(\mathrm{cc},1)}=\frac{1}{i\hbar}[(\hbar\Omega^{e}_{\mathbf{k}}+\hbar\Omega^{h}_{-\mathbf{k}})p_{\mathbf{k}}+\Delta_{\mathbf{k}}(1-f^{e}_{\mathbf{k}}-f^{h}_{-\mathbf{k}})] \tag{19}$$

with the self-energy of electrons and holes $\hbar\Omega^{e,h}_{\mathbf{k}}=-\Sigma_{\mathbf{k}'}V_{\mathbf{k}-\mathbf{k}'}f^{e,h}_{\mathbf{k}'}$ and the internal field $\Delta_{\mathbf{k}}=-\Sigma_{\mathbf{k}'}V_{\mathbf{k}-\mathbf{k}'}p_{\mathbf{k}'}$.

As for the case of cp interaction, scattering processes appear for the first time in the second-order contributions. For cc interaction they are obtained from the two-particle correlations, i.e., the deviations of the two-particle density matrices from their respective factorizations, e.g.,

$$\delta\langle c^{\dagger}_{\mathbf{k}}c^{\dagger}_{\mathbf{k}'+\mathbf{q}}c_{\mathbf{k}'}c_{\mathbf{k}-\mathbf{q}}\rangle=\langle c^{\dagger}_{\mathbf{k}}c^{\dagger}_{\mathbf{k}'}c_{\mathbf{k}'+\mathbf{q}}c_{\mathbf{k}-\mathbf{q}}\rangle+f^{e}_{\mathbf{k}}f^{e}_{\mathbf{k}'}\delta_{\mathbf{k}',\mathbf{k}-\mathbf{q}}. \tag{20}$$

In the equations of motion for these two-particle correlations a factorization and a Markov approximation are performed as in the case of cp interaction. Details and a discussion of the approximations are given in Appendix B. This leads to the second-order cc contributions in the equations of motion for distribution functions and polarization,

$$\left.\frac{d}{dt}f^{e}_{\mathbf{k}}\right|^{(\mathrm{cc},2)}=-\sum_{\mathbf{q}}[W^{e(\mathrm{cc})}_{\mathbf{k}-\mathbf{q},\mathbf{k}}f^{e}_{\mathbf{k}}-W^{e(\mathrm{cc})}_{\mathbf{k},\mathbf{k}-\mathbf{q}}f^{e}_{\mathbf{k}-\mathbf{q}}]+\frac{1}{i\hbar}[\Delta^{e(\mathrm{cc},2)}_{\mathbf{k}}p^{*}_{\mathbf{k}}-\Delta^{e(\mathrm{cc},2)*}_{\mathbf{k}}p_{\mathbf{k}}], \tag{21}$$

$$\left.\frac{d}{dt}f^{h}_{\mathbf{k}}\right|^{(\mathrm{cc},2)}=-\sum_{\mathbf{q}}[W^{h(\mathrm{cc})}_{\mathbf{k}-\mathbf{q},\mathbf{k}}f^{h}_{\mathbf{k}}-W^{h(\mathrm{cc})}_{\mathbf{k},\mathbf{k}-\mathbf{q}}f^{h}_{\mathbf{k}-\mathbf{q}}]+\frac{1}{i\hbar}[\Delta^{h(\mathrm{cc},2)}_{-\mathbf{k}}p^{*}_{-\mathbf{k}}-\Delta^{h(\mathrm{cc},2)*}_{-\mathbf{k}}p_{-\mathbf{k}}], \tag{22}$$

$$\left.\frac{d}{dt}p_{\mathbf{k}}\right|^{(\mathrm{cc},2)}=-\sum_{\mathbf{q}}[\mathscr{W}^{p(\mathrm{cc})}_{\mathbf{k}-\mathbf{q},\mathbf{k}}p_{\mathbf{k}}-\mathscr{W}^{p(\mathrm{cc})}_{\mathbf{k},\mathbf{k}-\mathbf{q}}p_{\mathbf{k}-\mathbf{q}}], \tag{23}$$

with

$$W^{e,h(\mathrm{cc})}_{\mathbf{k}-\mathbf{q},\mathbf{k}}=\frac{\pi}{\hbar}|V_{\mathbf{q}}|^{2}\sum_{\nu'=e,h}\sum_{\mathbf{k}'}\mathscr{D}(\epsilon^{e,h}_{\mathbf{k}-\mathbf{q}}+\epsilon^{\nu'}_{\mathbf{k}'+\mathbf{q}}-\epsilon^{\nu'}_{\mathbf{k}'}-\epsilon^{e,h}_{\mathbf{k}})\times[f^{\nu'}_{\mathbf{k}'}(1-f^{\nu'}_{\mathbf{k}'+\mathbf{q}})-p^{*}_{\mathbf{k}'+\mathbf{q}}p_{\mathbf{k}'}](1-f^{e,h}_{\mathbf{k}-\mathbf{q}})+\mathrm{c.c.}, \tag{24}$$

$$\mathscr{W}^{p(\mathrm{cc})}_{\mathbf{k}-\mathbf{q},\mathbf{k}}=\frac{\pi}{\hbar}|V_{\mathbf{q}}|^{2}\sum_{\nu,\nu'=e,h}\sum_{\mathbf{k}'}\mathscr{D}(\epsilon^{\nu}_{\mathbf{k}-\mathbf{q}}+\epsilon^{\nu'}_{\mathbf{k}'+\mathbf{q}}-\epsilon^{\nu'}_{\mathbf{k}'}-\epsilon^{\nu}_{\mathbf{k}})\times[-p^{*}_{\mathbf{k}'+\mathbf{q}}p_{\mathbf{k}'}+f^{\nu'}_{\mathbf{k}'}(1-f^{\nu'}_{\mathbf{k}'+\mathbf{q}})(1-f^{\nu}_{\mathbf{k}-\mathbf{q}})+f^{\nu}_{\mathbf{k}-\mathbf{q}}f^{\nu'}_{\mathbf{k}'+\mathbf{q}}(1-f^{\nu'}_{\mathbf{k}'})], \tag{25}$$

$$\Delta^{e,h(\mathrm{cc},2)}_{\mathbf{k}}=i\pi\sum_{\mathbf{k}',\mathbf{q}}\sum_{\nu'=e,h}|V_{\mathbf{q}}|^{2}\mathscr{D}(\epsilon^{h,e}_{\mathbf{k}}+\epsilon^{\nu'}_{\mathbf{k}'}-\epsilon^{\nu'}_{\mathbf{k}'+\mathbf{q}}-\epsilon^{h,e}_{\mathbf{k}-\mathbf{q}})\times[f^{\nu'}_{\mathbf{k}'+\mathbf{q}}-f^{\nu'}_{\mathbf{k}'}]p_{\mathbf{k}-\mathbf{q}}. \tag{26}$$

The structure of the second-order cc contributions is exactly the same as for cp interaction and again shows ''in-scattering'' and ''out-scattering'' terms both for distribution functions and polarization.

### D. Equations of motion

Including the various types of interactions up to the second order, the equations of motion for distribution functions and interband polarization can be summarized as

$$\frac{d}{dt}f^{e}_{\mathbf{k}}=g^{e}_{\mathbf{k}}(t)-\sum_{\mathbf{q}}[W^{e}_{\mathbf{k}-\mathbf{q},\mathbf{k}}f^{e}_{\mathbf{k}}-W^{e}_{\mathbf{k},\mathbf{k}-\mathbf{q}}f^{e}_{\mathbf{k}-\mathbf{q}}], \tag{27}$$

$$\frac{d}{dt}f^{h}_{\mathbf{k}}=g^{h}_{-\mathbf{k}}(t)-\sum_{\mathbf{q}}[W^{h}_{\mathbf{k}-\mathbf{q},\mathbf{k}}f^{h}_{\mathbf{k}}-W^{h}_{\mathbf{k},\mathbf{k}-\mathbf{q}}f^{h}_{\mathbf{k}-\mathbf{q}}], \tag{28}$$

$$\frac{d}{dt}p_{\mathbf{k}}=\frac{1}{i\hbar}(\mathscr{E}^{e}_{\mathbf{k}}+\mathscr{E}^{h}_{-\mathbf{k}})p_{\mathbf{k}}+\frac{1}{i\hbar}\mathscr{U}^{p}_{\mathbf{k}}(t)(1-f^{e}_{\mathbf{k}}-f^{h}_{-\mathbf{k}})-\sum_{\mathbf{q}}[\mathscr{W}^{p}_{\mathbf{k}-\mathbf{q},\mathbf{k}}p_{\mathbf{k}}-\mathscr{W}^{p}_{\mathbf{k},\mathbf{k}-\mathbf{q}}p_{\mathbf{k}-\mathbf{q}}], \tag{29}$$

with the generation rates

$$g^{e,h}_{\mathbf{k}}(t)=\frac{1}{i\hbar}[\mathscr{U}^{e,h}_{\mathbf{k}}p^{*}_{\mathbf{k}}-\mathscr{U}^{e,h*}_{\mathbf{k}}p_{\mathbf{k}}], \tag{30}$$

the renormalized energies of electrons and holes due do the Hartree-Fock terms

$$\mathscr{E}^{e,h}_{\mathbf{k}}=\epsilon^{e,h}_{\mathbf{k}}+\hbar\Omega^{e,h}_{\mathbf{k}}, \tag{31}$$

the renormalized fields for electrons, holes, and polarization due to second-order cp and first- and second-order cc interaction

$$\mathscr{U}^{e,h,p}_{\mathbf{k}}=M_{\mathbf{k}}E_{0}(t)e^{-i\omega_{L}t}+\Delta^{e,h,p}_{\mathbf{k}}, \tag{32}$$

and the transition matrices $W^{e,h}_{\mathbf{k}-\mathbf{q},\mathbf{k}}$ and $\mathscr{W}^{p}_{\mathbf{k}-\mathbf{q},\mathbf{k}}$ as defined for cp and cc scattering in the previous sections.

It should be noted that the way of collecting the terms in the equations of motion is not unique. Instead of using matrices $W^{e,h}_{\mathbf{k}-\mathbf{q},\mathbf{k}}$ and $\mathscr{W}^{p}_{\mathbf{k}-\mathbf{q},\mathbf{k}}$, in- and out-scattering rates might be used.[22] The present way makes the symmetries between in- and out-scattering both for distribution functions and polarization directly obvious, which will be the starting point for the numerical technique described below. A direct consequence of this symmetry is a conservation law for the total polarization $\Sigma_{\mathbf{k}}p_{\mathbf{k}}$ due to the scattering processes in complete analogy with the particle conservation due to scattering processes in the BTE. A decay of the polarization, i.e., a dephasing, is only related to the interplay between coherent rotation and the scattering processes.

The transition matrices $W^{e,h}_{\mathbf{k}-\mathbf{q},\mathbf{k}}$ for the distribution functions are real quantities, however, they are not necessarily positive definite if the polarization scattering due to cc interaction ($\propto p^{*}_{\mathbf{k}'+\mathbf{q}}p_{\mathbf{k}'}$) is included. The matrix $\mathscr{W}^{p}_{\mathbf{k}-\mathbf{q},\mathbf{k}}$ is a complex quantity. The real part

$$W^{p}_{\mathbf{k}-\mathbf{q},\mathbf{k}}=\mathrm{Re}\mathscr{W}^{p}_{\mathbf{k}-\mathbf{q},\mathbf{k}} \tag{33}$$

describes scattering processes leading to a dephasing of the polarization and the imaginary part describes second-order

contributions to the band-gap renormalization. In the numerical investigations presented here these energy shifts have been neglected since typically first-order (Hartree-Fock) renormalizations are more important. We have neglected furthermore all contributions in the transition matrices involving polarizations as well as the second-order contributions to the effective field. This is expected to be a good approximation for the case of excitation far from the gap where excitonic effects play a minor role.[30]

In contrast to the distribution functions, the polarization $p_{\mathbf{k}}(t)$ is a complex quantity with a phase depending on $\mathbf{k}$ and $t$. Therefore, it is often argued that when performing the $\mathbf{q}$ summation in the last term of Eq. (29), a cancellation occurs due to random phases and this term is negligible. Then a $\mathbf{k}$-dependent dephasing rate can be introduced according to

$$\Gamma_{\mathbf{k}}=\sum_{\mathbf{q}} W^{p}_{\mathbf{k}-\mathbf{q},\mathbf{k}}. \tag{34}$$

Physically, this approximation means that each scattering process completely destroys the pair coherence between electrons and holes, and the total scattering rate $\Gamma_{\mathbf{k}}$ plays the role of a $\mathbf{k}$-dependent dephasing rate. We will refer to this case as the dephasing-rate approximation.

Within the approximations discussed above, all transition matrices are positive-definite quantities and the incoherent parts for both distribution functions and polarization have the structure of rate equations with transition matrices $W^{e,h,p}_{\mathbf{k}-\mathbf{q},\mathbf{k}}$, the only difference being the complex nature of the polarization. This is the basis for the generalized Monte Carlo technique for the solution of the coupled set of equations of motion that will be discussed in the next section.

## III. NUMERICAL PROCEDURE

As discussed above, the aim of this paper is to extend the traditional Monte Carlo method for the solution of the Boltzmann equation[1,12] to the analysis of coherent phenomena, which are found to play a dominant role in the dynamic evolution of photoexcited semiconductors on short time scales. The main features that are not included in the traditional Monte Carlo method and that we want to take into account are the phase relations between different types of carriers (polarization phenomena), their interaction with an external coherent electromagnetic field (generation-recombination processes), and the correlation and renormalization effects associated with cc interaction (Hartree-Fock terms). As shown in Sec. II, in order to describe such coherent phenomena we need to solve the system of equations of motion (27)–(29) for the distribution functions and for the corresponding interband polarization, according to the interactions taken into account.

In order to see the limitations of a ''conventional'' Monte Carlo simulation and to discuss the problems arising when trying to generalize it, let us recall briefly the basic ideas of the traditional approach to semiclassical transport.

### A. The semiclassical limit and the conventional Monte Carlo simulation

The semiclassical limit is obtained by eliminating the polarization within the adiabatic and Markov approximations as described in Ref. 23 resulting in a semiclassical generation rate in Eqs. (27) and (28). Since the internal field is directly related to the polarization, it has to be neglected. Excitonic effects cannot be described in this limit. Apart from the generation terms (which in this limit can be regarded as an additional scattering mechanism from the valence to the conduction band), these semiclassical Boltzmann equations are of the general form

$$\frac{d}{dt}f_{\mathbf{k}}=\sum_{\mathbf{k}'}\left[W_{\mathbf{k},\mathbf{k}'}f_{\mathbf{k}'}-W_{\mathbf{k}',\mathbf{k}}f_{\mathbf{k}}\right], \tag{35}$$

where each $\mathbf{k}$ denotes a certain region of the phase space and $f_{\mathbf{k}}$ its average occupation number. The explicit form of the scattering rates $W_{\mathbf{k},\mathbf{k}'}$ depends on the interaction mechanisms considered as discussed in Sec. II. In general, they depend on the distribution function itself. Therefore, the scattering rates become time dependent via the time dependence of the distribution functions and we deal with a system of nonlinear equations. In order to treat these nonlinearities, a fixed time step is usually introduced, at the end of which the new distribution functions are evaluated so that the new scattering rates can be determined. In this way, within each time step, we deal with a system of linear equations: The scattering rates are fixed quantities and the individual carriers can evolve asynchronously.

Let us consider the semiclassical Boltzmann equation (35) over a single time step, i.e., from time $t_0$ to time $t_0+\Delta t$. Due to the local linearity of the transport equation, the distribution function $f_{\mathbf{k}}$ at time $t$ $(t_0<t<t_0+\Delta t)$ can be written as

$$f_{\mathbf{k}}(t)=\sum_{\mathbf{k}'} G_{\mathbf{k},\mathbf{k}'}(t,t_0)f_{\mathbf{k}'}(t_0), \tag{36}$$

where the Green's function $G$, called Boltzmann propagator, has a direct physical interpretation: It describes the probability that a particle in state $\mathbf{k}'$ at time $t_0$ will be found in state $\mathbf{k}$ at time $t$. From its definition, the Boltzmann propagator must be also a solution of the Boltzmann equation (35) and it must satisfy the initial condition

$$G_{\mathbf{k},\mathbf{k}'}(t_0,t_0)=\delta_{\mathbf{k},\mathbf{k}'}. \tag{37}$$

It is therefore clear that all the information concerning the system dynamics is contained in the above Boltzmann propagator. The state of the system at time $t$ is the result of the independent evolution of the initial condition $f_{\mathbf{k}'}(t_0)$ (i.e., the initial set of carriers) through the propagator $G$. The sum over $\mathbf{k}$ space can be replaced by a direct sum over an appropriate ensemble of simulative carriers:

$$\begin{aligned} f_{\mathbf{k}}(t)&=\sum_{\mathbf{k}'} G_{\mathbf{k},\mathbf{k}'}(t,t_0)f_{\mathbf{k}'}(t_0)\approx\sum_{\mathbf{k}'}\sum_{i=1}^{N_{\mathbf{k}'}} G_{\mathbf{k},\mathbf{k}'}(t,t_0)w \\ &=\sum_{i=1}^{N} G_{\mathbf{k},\mathbf{k}_i}(t,t_0)w, \end{aligned} \tag{38}$$

where $N_{\mathbf{k}'}$ denotes the number of simulative carriers representing $f_{\mathbf{k}'}$, $w$ is the weight of each simulative carrier, $\mathbf{k}_i$ denotes the state of the $i$th carrier at time $t_0$, and $N=\Sigma_{\mathbf{k}'}N_{\mathbf{k}'}$ is the total number of simulative carriers. From the above equation we see that the distribution function at

time $t$ can be simply written as the sum of the Boltzmann propagators corresponding to each carrier in the system and, in particular, we see that the weight of all the propagators in the sum is the same. In addition, we want to stress that the Boltzmann propagator is a real and positive-definite quantity. We will come back to this crucial point later.

Equation (38) can be regarded as the starting point of the traditional ensemble Monte Carlo (EMC) technique,[12] which simply provides a Monte Carlo sampling of the sum. Such sampling is performed by means of a stochastic simulation of a suitable ensemble of $N$ carriers. However, they do not correspond to the real physical particles of the system. For each simulative carrier, a sequence of random ''free flights,'' interrupted by random ''scattering events,'' is generated. Such a ''random walk'' in $\mathbf{k}$ space is just a Monte Carlo sampling of the Boltzmann propagator $G_{\mathbf{k}_f,\mathbf{k}_i}(t,t_0)$, where $\mathbf{k}_i$ and $\mathbf{k}_f$ denote, respectively, the initial and the final state of the generic random walk.[31]

From the above considerations we see that the EMC technique, usually considered as a ''real'' direct simulation of the carrier dynamics, can be regarded from a more general point of view as a formal Monte Carlo sampling of the solution of the Boltzmann transport equation. As discussed in detail in Ref. 31, the conventional EMC technique is only a particular case of a more general approach, the weighted ensemble Monte Carlo method. This more general way of looking at the Monte Carlo simulation does not at all require the existence of ''real particles.'' The fictitious particles within the Monte Carlo simulation can be simply regarded as a mathematical instrument used in performing the statistical sampling of the physical quantity of interest. This result opens the way to extend the application of the Monte Carlo method to the evaluation of physical quantities different from the usual distribution function $f_{\mathbf{k}}$ of semiclassical particles.

### B. General structure of the kinetic equations

Let us now come back to the system of kinetic equations (27)–(29) discussed in Sec. II. As already discussed, the various kinetic equations exhibit a strong formal similarity: The contributions to the dynamics can be always split into a coherent and an incoherent contribution. Denoting by $\mathscr{F}_{\mathbf{k}}^{\alpha}$ the generic kinetic variable ($\alpha=e,h,p$) with $\mathscr{F}_{\mathbf{k}}^{e,h}\equiv f_{\mathbf{k}}^{e,h}$ and $\mathscr{F}_{\mathbf{k}}^{p}\equiv p_{\mathbf{k}}$, the system of equations (27)–(29) can be schematically written as

$$\frac{d}{dt}\mathscr{F}_{\mathbf{k}}^{\alpha}=\left.\frac{d}{dt}\mathscr{F}_{\mathbf{k}}^{\alpha}\right|_{\mathrm{co}}+\left.\frac{d}{dt}\mathscr{F}_{\mathbf{k}}^{\alpha}\right|_{\mathrm{inco}},\quad \alpha=e,h,p \tag{39}$$

with

$$\left.\frac{d}{dt}\mathscr{F}_{\mathbf{k}}^{\alpha}\right|_{\mathrm{co}}=\mathscr{C}_{\mathbf{k}}^{\alpha,0}(\{\mathscr{F}^{\alpha}\})+\sum_{j}\mathscr{C}_{\mathbf{k}}^{\alpha,j}(\{\mathscr{F}^{\alpha}\}), \tag{40}$$

$$\left.\frac{d}{dt}\mathscr{F}_{\mathbf{k}}^{\alpha}\right|_{\mathrm{inco}}=\sum_{j}\sum_{\mathbf{k}'}[W_{\mathbf{k},\mathbf{k}'}^{\alpha,j}\mathscr{F}_{\mathbf{k}'}^{\alpha}-W_{\mathbf{k}',\mathbf{k}}^{\alpha,j}\mathscr{F}_{\mathbf{k}}^{\alpha}], \tag{41}$$

where $W_{\mathbf{k},\mathbf{k}'}^{\alpha,j}$ denotes the scattering rate associated with the kinetic variable $\alpha$ for a transition $\mathbf{k}'\rightarrow\mathbf{k}$ induced by the $j$th interaction mechanism and $\mathscr{C}_{\mathbf{k}}^{\alpha,j}$ is some functional of the kinetic variables whose explicit form has been discussed in Sec. II.

Equation (39) is again a system of nonlinear equations. Therefore, as in the semiclassical case, we introduce a time discretization in terms of a fixed time step $\Delta t$. By integrating Eq. (39) over $\Delta t$, we obtain

$$\mathscr{F}_{\mathbf{k}}^{\alpha}(t_0+\Delta t)=\mathscr{F}_{\mathbf{k}}^{\alpha}(t_0)+\Delta.\mathscr{F}_{\mathbf{k}}^{\alpha}|_{\mathrm{co}}+\Delta.\mathscr{F}_{\mathbf{k}}^{\alpha}|_{\mathrm{inco}},\quad \alpha=e,h,p. \tag{42}$$

Therefore, the time variation of the generic kinetic variable $\mathscr{F}$ over the time step results in the sum of two independent contributions: the coherent and the incoherent one. In the numerical procedure, for each time step, the coherent contributions are evaluated by means of a direct numerical integration while the incoherent contributions are ''sampled'' by means of a generalized Monte Carlo simulation.

### C. Generalized Monte Carlo simulation

Let us focus our attention on the explicit form of the incoherent contributions given in Eq. (41). Within the approximations discussed in Sec. II D they have exactly the structure of the ''Boltzmann collision term.'' Denoting with

$$W_{\mathbf{k},\mathbf{k}'}^{\alpha}=\sum_{j}W_{\mathbf{k},\mathbf{k}'}^{\alpha,j} \tag{43}$$

the total scattering rate associated to the kinetic variable $\alpha$ for a transition from state $\mathbf{k}'$ to state $\mathbf{k}$, Eq. (41) can be written as

$$\left.\frac{d}{dt}\mathscr{F}_{\mathbf{k}}^{\alpha}\right|_{\mathrm{inco}}=\sum_{\mathbf{k}'}[W_{\mathbf{k},\mathbf{k}'}^{\alpha}\mathscr{F}_{\mathbf{k}'}^{\alpha}-W_{\mathbf{k}',\mathbf{k}}^{\alpha}\mathscr{F}_{\mathbf{k}}^{\alpha}]. \tag{44}$$

We want to stress that in the present approximation for all kinetic variables (including the polarization, i.e., $\alpha=p$) the various $W_{\mathbf{k},\mathbf{k}'}^{\alpha}$ are positive-definite quantities, i.e., they can be regarded as ''true'' scattering probabilities from state $\mathbf{k}'$ to state $\mathbf{k}$.

Thus, the ''generalized Boltzmann equation'' (44) for the kinetic variables $\mathscr{F}^{\alpha}$ has exactly the same structure as the semiclassical Boltzmann equation (35), apart from the fact that the kinetic variable $\mathscr{F}^{\alpha}$, in general, is a complex quantity. This fact, however, does not limit the application of the Monte Carlo method in its general formulation. Due to the local linearity of our transport equation within one time step, the kinetic variable $\mathscr{F}_{\mathbf{k}}^{\alpha}$ at time $t$ ($t_0<t<t_0+\Delta t$) can be written as

$$\mathscr{F}_{\mathbf{k}}^{\alpha}(t)=\sum_{\mathbf{k}'}G_{\mathbf{k},\mathbf{k}'}^{\alpha}(t,t_0).\mathscr{F}_{\mathbf{k}'}^{\alpha}(t_0), \tag{45}$$

where $G^{\alpha}$ is now a generalized Boltzmann propagator corresponding to the kinetic variable $\alpha$. As in the semiclassical case, the propagator $G^{\alpha}$ must be a solution of the generalized Boltzmann equation (44) and it must verify the initial condition (37). Again, all the information concerning the dynamics is contained in the real quantity $G^{\alpha}$. The state of the

system at time $t$ is the result of the independent evolution of the initial condition $\mathscr{F}^{\alpha}_{\mathbf{k}'}(t_0)$ through the corresponding propagator.

Equation (45) constitutes the starting point of our generalized Monte Carlo approach, which, by itself, simply provides a Monte Carlo sampling of the sum in Eq. (45). As in the semiclassical case, such a sampling is performed by means of a stochastic simulation of a suitable ensemble of $N$ carriers, which, in general, have nothing to do with real physical particles. At the initial time $t_0$ the ensemble of $N$ particles is assumed to be distributed in $\mathbf{k}$ space according to the absolute value of the kinetic variable $\mathscr{F}^{\alpha}_{\mathbf{k}}$:

$$N^{\alpha}_{\mathbf{k}}(t_0)=C^{\alpha}|\mathscr{F}^{\alpha}_{\mathbf{k}}(t_0)|, \tag{46}$$

where $C^{\alpha}$ is a normalization coefficient.

The sum over $\mathbf{k}$ space in Eq. (45) can then be translated into a sum over this ensemble of simulative carriers:

$$\mathscr{F}^{\alpha}_{\mathbf{k}}(t)=\sum_{\mathbf{k}'} G^{\alpha}_{\mathbf{k},\mathbf{k}'}(t,t_0)w^{\alpha}_{\mathbf{k}'}N^{\alpha}_{\mathbf{k}'}(t_0)=\sum_{j=1}^{N} G^{\alpha}_{\mathbf{k},\mathbf{k}_j}(t,t_0)w^{\alpha}_{j}, \tag{47}$$

where

$$w^{\alpha}_{j}=\frac{1}{C^{\alpha}}\frac{\mathscr{F}^{\alpha}_{\mathbf{k}_j}(t_0)}{|\mathscr{F}^{\alpha}_{\mathbf{k}_j}(t_0)|}=W^{\alpha}e^{i\phi^{\alpha}_{j}} \tag{48}$$

can be regarded as a ''weight'' of the $j$th simulative particle in the sum. As in the semiclassical case, its absolute value $W^{\alpha}$ is the same for all the particles but its phase $\phi^{\alpha}_{j}$ is that of the kinetic variable $\mathscr{F}^{\alpha}_{\mathbf{k}_j}$ from which the simulative carrier originates. Therefore, the function $\mathscr{F}^{\alpha}_{\mathbf{k}}$ at time $t$ is given by the sum of the Boltzmann propagators related to the various simulative carriers, each one multiplied by its weight $w^{\alpha}_{j}$. In order to evaluate the Boltzmann propagator $G^{\alpha}$, the conventional EMC simulation discussed in Sec. III A can be employed.

Our generalized Monte Carlo sampling proceeds as follows: Given the initial condition $\mathscr{F}^{\alpha}_{\mathbf{k}}$, an ensemble of $N$ simulative carriers is randomly generated in $\mathbf{k}$ space according to the absolute value of $\mathscr{F}^{\alpha}_{\mathbf{k}}$ and to each carrier we attach a phase $\phi^{\alpha}_{j}$ defined in Eq. (48). For each simulative carrier, a sequence of random ''free flights,'' interrupted by random ''scattering events,'' is then generated according to the scattering rates $W^{\alpha}_{\mathbf{k},\mathbf{k}'}$. As for the semiclassical case, it can be shown[31] that such ''random walk'' in $\mathbf{k}$ space is just a Monte Carlo sampling of the Boltzmann propagator $G^{\alpha}_{\mathbf{k}_f,\mathbf{k}_i}(t,t_0)$. The desired kinetic variable $\mathscr{F}^{\alpha}_{\mathbf{k}}$ at time $t$ is finally obtained by summing the phase factors $w^{\alpha}_{j}=W^{\alpha}e^{i\phi^{\alpha}_{j}}$ of all the simulative carriers that at time $t$ are in state $\mathbf{k}$. When the kinetic variable is a distribution function (i.e., $\alpha=e$ or $\alpha=h$), all the phases $\phi^{\alpha}_{j}$ are equal to zero. Therefore, the above summation simply reduces to the usual ''counting'' of the particles in state $\mathbf{k}$ and the conventional EMC technique is recovered.

Finally, we want to stress that the random generation of the initial distribution of simulative carriers according to the absolute value of $\mathscr{F}^{\alpha}_{\mathbf{k}}$ is only one of very many possibilities. However, this is the only one for which all carriers have the same weight $W^{\alpha}$ apart from the phase $\phi^{\alpha}_{j}$. This provides, in general, a strong reduction of the statistical fluctuations. This particular choice can then be regarded, to some extent, as a sort of ''generalized importance sampling.''[32]

The structure of the numerical procedure can then be summarized as follows: The total time is divided into time steps. The simulation starts at the initial time $t_i$ before the laser has been switched on. The system is chosen to be in its fundamental state, i.e., the vacuum of electron-hole pairs. The simulation then results in a loop over the various time steps and for each time step: (i) we evaluate the coherent contributions by means of a direct numerical integration; (ii) for each kinetic variable $\mathscr{F}^{\alpha}$, we introduce an ensemble of $N$ ''simulative particles'' according to $|\mathscr{F}^{\alpha}_{\mathbf{k}}|$ where we attach to each ''particle'' a phase factor $w^{\alpha}_{j}$ according to the phase of $\mathscr{F}^{\alpha}_{\mathbf{k}_j}$; (iii) for each of these ''particles'' we perform a traditional Monte Carlo simulation, i.e., a random sequence of ''free flights'' and ''scattering events'' originated by the scattering rates $W^{\alpha}_{\mathbf{k},\mathbf{k}'}$ in Eq. (44).

The generalized Monte Carlo approach described above has also been recently applied to the analysis of four-wave-mixing experiments.[33,34] In this case, a Monte Carlo simulation of the various, in general complex, Fourier components of the distribution functions is required.

## IV. APPLICATIONS

By applying the numerical procedure described in the previous section, we now analyze the generation and relaxation dynamics of laser-pulse excited carriers. First, we study the dynamics of the carrier distribution functions as obtained from the three different models: BTE, SBE in dephasing rate approximation, and SBE including the full scattering dynamics of the polarization. In order to get more insight into the failure of the dephasing-rate approximation, in particular at low densities, we then investigate the $\mathbf{k}$ space dynamics of the polarization. If not stated explicitly, all simulations refer to a Gaussian laser pulse with amplitude $E_0(t)=E_L\exp(-t^2/\tau_L^2)$, a width $\tau_L=85$ fs (corresponding to a full width at half maximum of the intensity of 100 fs) and an excess energy of 180 meV. The GaAs material parameters used for all simulations can be found in Ref. 23.

In Fig. 1 the electron energy distribution $\sqrt{\epsilon^{e}_{\mathbf{k}}}f^{e}_{\mathbf{k}}$ at time $t=100$ fs, i.e., towards the end of the pulse, is plotted as a function of the electron energy for the three models at three different densities. In the BTE case [Fig. 1(a)] at the lowest density we see the peak of the generated carriers at 160 meV and, at lower energies, replicas due to the emission of an integer number of optical phonons. The width of the peaks is given by the width of the laser pulse, cc scattering plays essentially no role at this low density. With increasing density cc scattering becomes more efficient, resulting in an increased broadening of the peaks. Due to band-gap renormalization, at a density of $10^{18}$ cm$^{-3}$ the generated peak is shifted towards higher energies. In the SBE case in the dephasing rate approximation [Fig. 1(b)] the behavior is completely different. It turns out that here the broadening is determined by the scattering terms in the polarization equation. We observe distribution functions with nearly the same

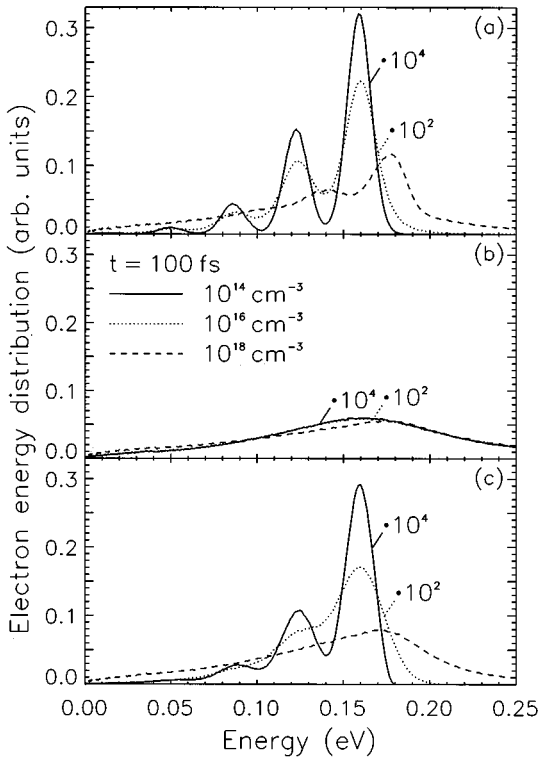


FIG. 1. Electron energy distribution at different densities for the case of excitation with an 85-fs pulse at $t = 100$ fs obtained from (a) the Boltzmann model, (b) the Bloch model without in-scattering terms in the polarization equation, and (c) the full Bloch model.

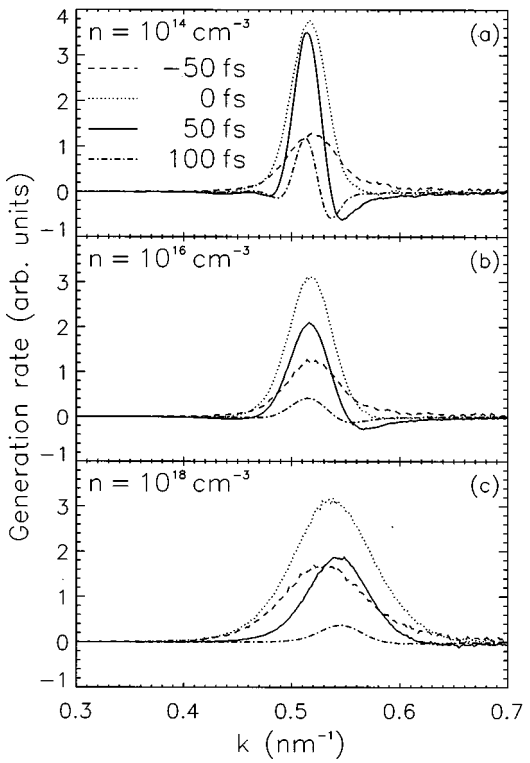


FIG. 2. Generation rates for the case of excitation with an 85-fs laser pulse at different times and densities obtained from the full Bloch model.

shape when varying the density over four orders of magnitude. This behavior, which is clearly unphysical, is related to the fact that the total cc scattering rate is nearly density independent. The increase in the number of partner carriers for a scattering process is almost exactly compensated by the increase in the screening wave vector. However, the characteristic features of a scattering process change: At low densities scattering processes occur mainly in the forward direction. With increasing density the momentum exchange increases. In the equation for the distribution functions this leads to the strong density dependence as observed in Fig. 1(a). However, in the equation of motion for the polarization this phenomenon is completely neglected if the dephasing is described only in terms of the total scattering rate. Including the in-scattering terms in the SBE model [Fig. 1(c)], we recover the correct low-density limit where, as observed experimentally,[16,35,36] phonon replicas are present. Compared with the BTE case, at $10^{14}$ cm$^{-3}$ the peaks are slightly broader, which is due mainly to cp scattering in the polarization equation. With increasing density the SBE results exhibit a much more pronounced broadening than the BTE case because of the increased efficiency of cc scattering processes both in the equations for the distribution functions and in the equation for the polarization. It turns out that the latter one gives the dominant contribution due to the fact that while in the BTE case the electron distribution is influenced only by scattering processes of the electrons, the dynamics of the polarization involves scattering processes of electrons and holes, the latter ones being more important due to their larger density of states. At the highest density no more phonon-related structure is observable, in contrast to the BTE case. However, it is noteworthy that even at the density of $10^{18}$ cm$^{-3}$ there is still a remarkable difference between the SBE cases (b) and (c), in particular on the high-energy tail, showing that the dephasing rate approximation still overestimates the scattering efficiency.

The increasing difference between BTE and SBE when increasing the density can be understood by looking at the generation rate at different times as plotted in Fig. 2. In the BTE case the generation rate is completely determined by the spectral profile of the laser pulse. Therefore the shape of the generation rate is constant in time, only its amplitude follows the intensity of the laser pulse. In contrast, in the SBE case carrier generation is determined by the dynamics of the polarization, which is strongly influenced by scattering processes and therefore it becomes density dependent. As discussed in detail in Ref. 23 for the case without cc scattering, as a consequence of the energy-time uncertainty the width of the generation rate decreases with increasing time, exhibiting negative parts off-resonance due to stimulated recombination processes. These recombination processes, however, require a coherence to be still present in the carrier system. An increasing density leads to an increased efficiency of cc scattering and, therefore, to a loss of coherence. Thus, stimulated recombination processes are inhibited and the generation rate remains broad, resulting in a much broader generation of the carriers than in the semiclassical case. Figure 2(c) clearly shows the shift of the generation rate towards higher energies during the buildup of the carrier distribution due to the increase in the band-gap renormalization.

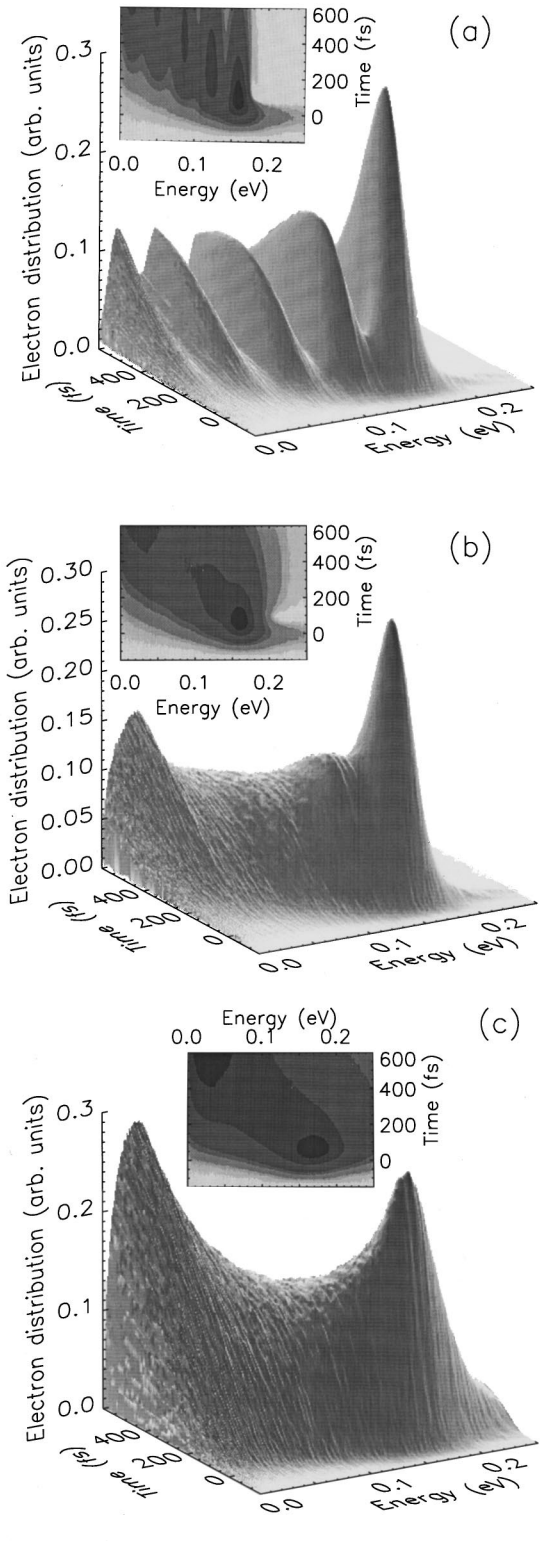


FIG. 3. Evolution of the electron energy distribution after excitation with an 85-fs laser pulse obtained from the full Bloch model showing relaxation due to (a) mainly cp interaction (final density $n=10^{14}$ cm$^{-3}$), (b) cc and cp interaction (final density $n=10^{16}$ cm$^{-3}$, and (c) mainly cc interaction (final density $n=10^{18}$ cm$^{-3}$).

Figure 3 summarizes the generation and relaxation dynamics of the electron distribution function as a function of energy and time for the three densities discussed above as obtained from the full SBE model. At the lowest density the subsequent buildup of the phonon replicas is clearly visible. At the intermediate density the first replica is still visible, however, due to cc scattering it is already strongly broadened. At the highest density no more phonon-related structures are observable; the electron distribution relaxes continously towards the band edge. Looking at the contour plots one can see in particular in the low-density case the successive buildup of the electron energy distribution. The width of the carrier distribution is reduced due to the stimulated recombination discussed above. Comparing the insets for the three different densities, we clearly see an increase of the linewidth with increasing density.

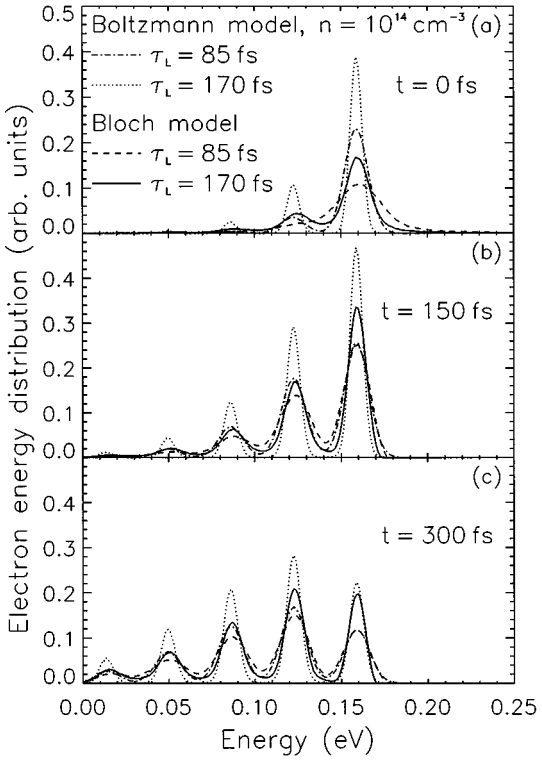


FIG. 4. Electron energy distribution at low density for two different pulse durations obtained from the BTE and the SBE model.

The differences between the BTE and the SBE approaches depend also on the pulse duration. To analyze this dependence, in Figs. 4 and 5 we compare the electron energy distributions at three different times obtained by a 85-fs pulse with those obtained by a 170-fs pulse. Figure 4 shows the results for low density ($10^{14}$ cm$^{-3}$). At $t=0$ fs we find pronounced differences between BTE and SBE results for both pulse widths due to the fact that, as discussed above, in the SBE approach at the center of the pulse energy-time uncertainty leads to a broadening that is twice as big as that obtained from the total pulse duration. In the absence of efficient dephasing processes, with increasing time the broadening in the SBE case decreases, resulting in much more similar distributions after the pulse [Fig. 4(c)]. It is interesting to notice that the agreement is better for the generated peak than for the phonon replicas due to the fact that carriers in the phonon replicas have been generated at earlier times. Furthermore, we find a slightly better agreement for the short pulse than for the long pulse mainly related to a

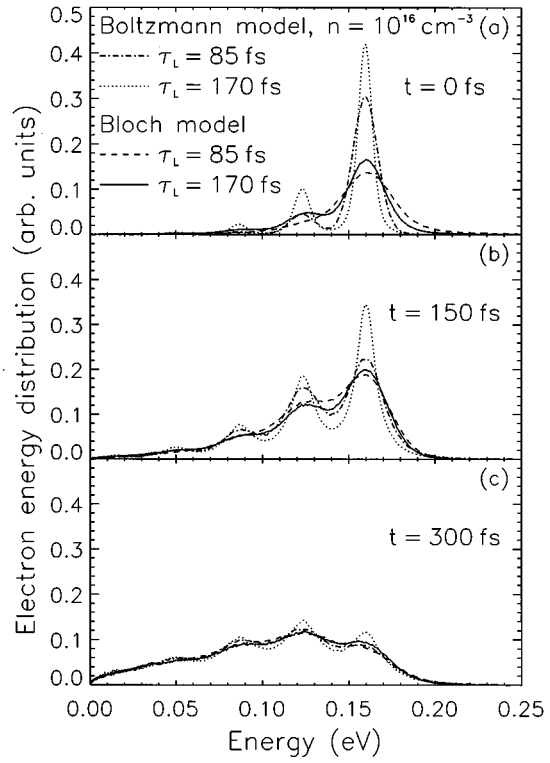


FIG. 5. Same as Fig. 4 but at an intermediate density.

small broadening due to the dephasing by cp scattering processes, which is observable only if the pulse width becomes of the order of the cp scattering time.

At the higher density ($10^{16}$ cm$^{-3}$, Fig. 5) the influence of the pulse width becomes much more pronounced. In the BTE case the energetic width of the generation rate is determined by the laser pulse. Thus, for the longer pulse we find much narrower peaks than for the shorter pulse. Due to the narrow generation rate we still find pronounced phonon replicas at $t=300$ fs. The broadening of the distribution function occurs mainly by a growing background, while the width of the generated peak and its replicas increases only slightly. In the SBE case, on the other hand, at this density the energetic width of the generation rate is determined by dephasing processes and therefore it is essentially the same for both pulses. At all times there is nearly no dependence of the distribution functions on the pulse duration. Here it is clearly evident that the main origin of the broadening of the distribution function is not related to scattering processes of the generated carriers but to the broadening of the generation process itself. In particular, the phonon replicas that are present in the BTE case for the longer pulse are strongly washed out.

The results discussed above have demonstrated the importance of the dynamics of the interband polarization on the shape of the carrier distributions. Therefore, now we concentrate on the density dependence of the dynamics of the polarization. In Fig. 6 the real and imaginary parts are plotted as functions of wave vector and time. Here, the fast oscillation related to the laser frequency has been taken out; i.e., we have plotted the real and imaginary parts of $p_{\mathbf{k}}\exp(i\omega_L t)$. The real parts exhibit a dispersive behavior with zero at resonance and the imaginary parts exhibit a mainly absorptive behavior characterized by negative values centered around

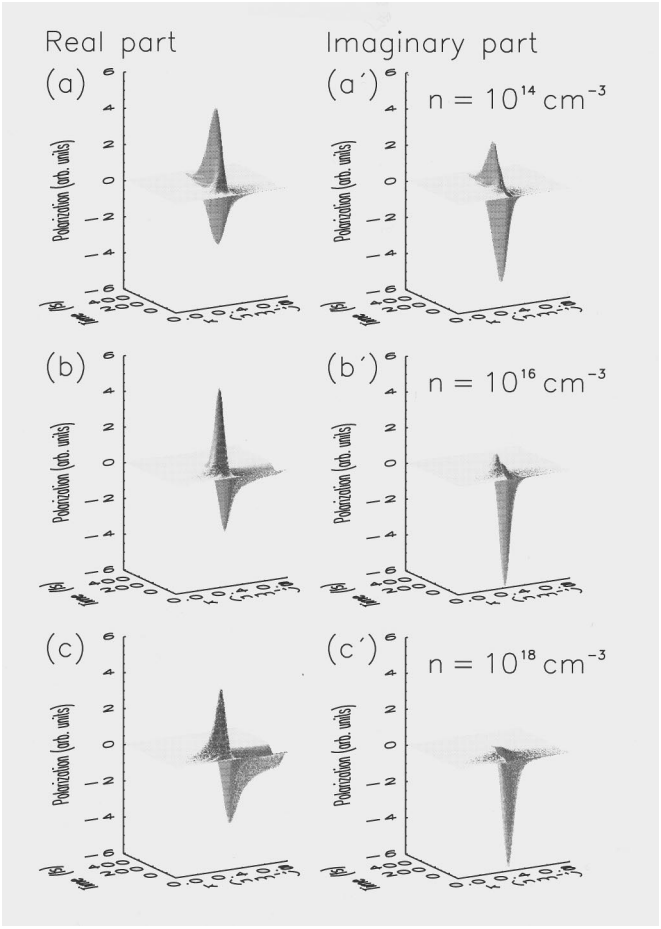


FIG. 6. Real and imaginary parts of the interband polarization as functions of wave vector and time for three different densities.

resonance. At low densities the imaginary part has positive values off-resonance that are responsible for the stimulated recombination resulting finally in the narrow generation rate. With increasing density these positive parts are reduced in agreement with the reduction of negative parts in the generation rate as discussed above (see Fig. 2). Furthermore, by looking at the time decay of the polarization, we observe a strong increase in the dephasing with increasing density as is expected due to the increased efficiency of cc scattering. It should be mentioned that, again, from a dephasing-rate approximation we would find a very fast decay of the polarization that is nearly density independent.

The dynamics of the polarization allows us to obtain a deeper insight into the question of why the dephasing rate approximation leads to completely unphysical results, in particular at low densities. For this purpose the scattering part of the equation of motion for the polarization may be written as

$$\frac{d}{dt}p_{\mathbf{k}}=R_{\mathbf{k}}p_{\mathbf{k}}=\sum_{\mathbf{q}}\left(-W^{p}_{\mathbf{k}-\mathbf{q},\mathbf{k}}+W^{p}_{\mathbf{k},\mathbf{k}-\mathbf{q}}\frac{p_{\mathbf{k}-\mathbf{q}}}{p_{\mathbf{k}}}\right)p_{\mathbf{k}}. \quad (49)$$

In this notation, the quantity $R_{\mathbf{k}}=|R_{\mathbf{k}}|\exp(i\Delta\varphi_{\mathbf{k}})$ can be interpreted as a generalized rate, which, however, is a complex variable with modulus and phase. In the dephasing rate approximation the second term in the brackets is neglected and the modulus coincides with the total scattering rate $\Gamma_{\mathbf{k}}$. The phase is independent of $\mathbf{k}$ and equal to $\pi$. Due to the struc-

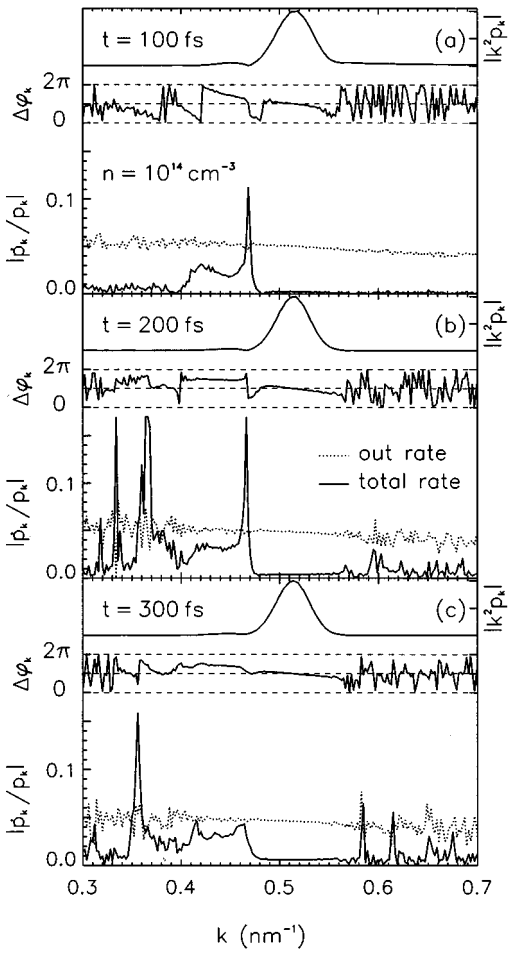


FIG. 7. Complex ''scattering rates'' for the polarization (see text) for a final density of $n=10^{14}$ cm$^{-3}$ at different times. At each time the figure shows the $\mathbf{k}$ dependence of the polarization $|k^2 p_{\mathbf{k}}|$, the absolute value of the rate of change $|R_{\mathbf{k}}|$, and the phase difference $\Delta\varphi_{\mathbf{k}}$ between in- and out-scattering terms.

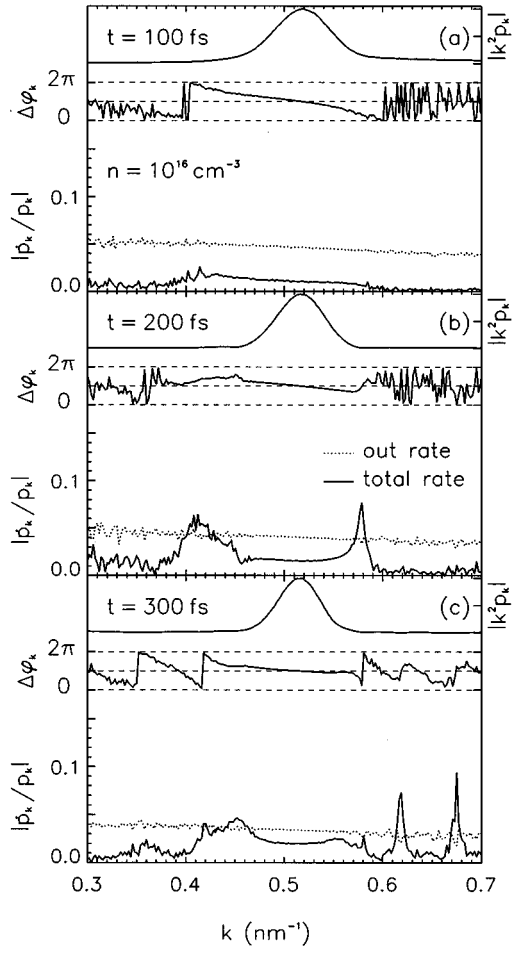


FIG. 8. Same as Fig. 7 but for a final density of $n=10^{16}$ cm$^{-3}$.

ture of the equation, we will refer to this case as to the out rate. In the full model, on the other hand, depending on the relative phases of $p_{\mathbf{k}}$ and $p_{\mathbf{k}-\mathbf{q}}$, both modulus and phase become $\mathbf{k}$ dependent. The modulus indicates the scattering efficiency and the phase determines whether the polarization at a given wave vector is reduced (for $\Delta\varphi_{\mathbf{k}}\approx\pi$) or increased (for $\Delta\varphi_{\mathbf{k}}\approx 0$ or $2\pi$). The latter case describes polarization transfer between different regions in $\mathbf{k}$ space. In Figs. 7–9 we analyze the details of the scattering dynamics of the polarization by plotting modulus and phase of $R_{\mathbf{k}}$ at different times for the same three densities as above. In addition, we have included the modulus of the polarization including a density-of-states factor $|k^2 p_{\mathbf{k}}|$ in order to indicate the $\mathbf{k}$ region that is relevant for the dynamics.[37]

In the case of the lowest density ($10^{14}$ cm$^{-3}$, Fig. 7) we notice a big difference between the out rate and the total rate in the region of the generated polarization around $k=0.51$ nm$^{-1}$. This difference is clearly the reason for the failure of the dephasing rate approximation at low densities as seen in Fig. 1. The out rate (dotted line) is dominated by cc scattering. However, due to the weak screening the scattering matrix $W_{\mathbf{k},\mathbf{k}-\mathbf{q}}$ is strongly peaked around small $\mathbf{q}$ values. Therefore, the fraction $p_{\mathbf{k}-\mathbf{q}}/p_{\mathbf{k}}$ in Eq. (49) is approximately unity in the region of interest and the two contributions nearly cancel. The phase is always close to $\pi$ in this region, showing that, as expected, there is still dephasing, mainly due to cp scattering. It is interesting to notice that around $k=0.43$ nm$^{-1}$ the total rate is much larger than in the generated region and the phase differs significantly from $\pi$. This phenomenon is related to cp scattering: Like in the case of the electron distribution, where phonon replicas are created by the transfer of carriers in $\mathbf{k}$ space, the in-scattering term in Eq. (49) transfers polarization from the generation region to the $\mathbf{k}$ region of the first phonon replica. Due to the phase difference between initial and final polarization and the additional dephasing, however, this effect is much weaker than in the case of the distribution function. Nevertheless, it is responsible for a weak phonon-assisted generation at the first phonon replica.

With increasing density ($10^{16}$ cm$^{-3}$, Fig. 8) the screening wave vector increases, resulting in a less pronounced peaked shape of the scattering matrix. The $\mathbf{q}$ summation then extends over a larger range and the varying phase of the polarization results in a reduction of the in-scattering term. At the highest density ($10^{18}$ cm$^{-3}$, Fig. 9) the assumption of random phases in the in-scattering term is well satisfied, in particular at later times, where the total rate agrees practically

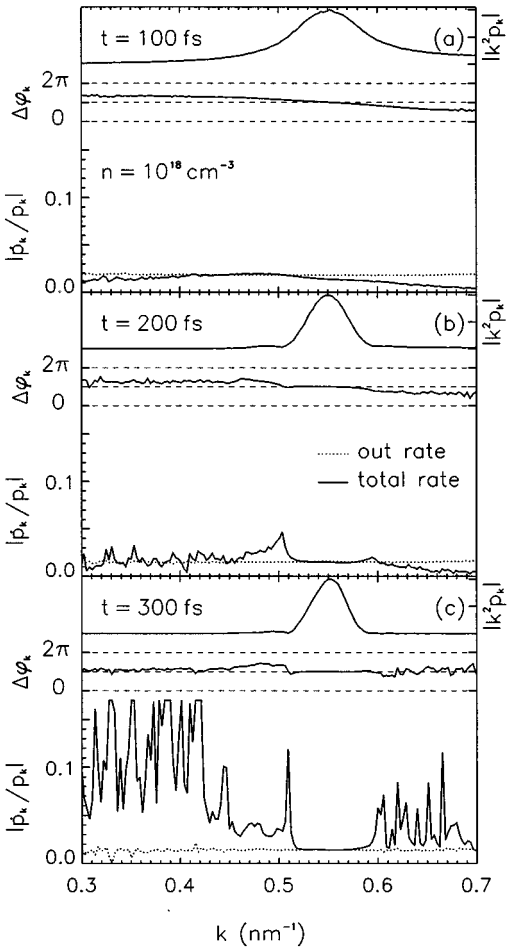


FIG. 9. Same as Fig. 7 but for a final density of $n=10^{18}$ $cm^{-3}$.

exactly with the out rate in the region of nonzero polarization. The big fluctuations at later times outside this region are due to numerical noise created by the very small denominator in Eq. (49) and is irrelevant for the dynamics. At early times, however, on the high-energy side there is still a strong cancellation between in- and out-scattering terms, which is responsible for the difference between full model and dephasing rate approximation in this region as found in Fig. 1.

## V. CONCLUSIONS

We have presented both the theoretical background and the technical aspects of a generalized Monte Carlo method recently proposed by the authors for the analysis of the mutually coupled coherent and incoherent phenomena characterizing the ultrafast carrier dynamics in photoexcited semiconductors. This approach combines on the same kinetic level the direct-integration method for the analysis of coherent dynamics with the Monte Carlo simulation for the study of the incoherent scattering regime.

This method has been applied to the study of the ultrafast carrier dynamics in pulse excited semiconductors based on a SBE approach including cc and cp interactions. It turned out that a dephasing rate approximation, where each scattering process completely destroys the phase coherence, strongly overestimates the dephasing at low and intermediate densities by producing very broad carrier distributions which are in clear contrast to experimental findings. Including contributions with the structure of in-scattering terms also in the polarization equation removes this unphysical behavior.

From the **k**-space dynamics of the polarization we have extracted a generalized complex ''dephasing rate,'' which clearly showed the cancelation between in- and out-scattering contributions at low densities and the existence of polarization transfer due to cp interaction. Thus, the scattering dynamics of the polarization exhibits a strong similarity with the scattering dynamics of the distribution functions. The difference, which eventually results in a decay of the polarization in contrast to the carrier conservation in the equation for the distribution function, is related to the complex nature of the polarization and the interplay between coherent rotation and scattering processes.

The present calculations have been performed with a statically screened Coulomb potential. On the time scale of a few tens of femtoseconds this might lead to an overestimation of the screening efficiency since the time required to build up the screening is neglected. As a consequence, the total scattering rate $\mathbf{\Gamma}_{\mathbf{k}}$ at very short times might be larger. However, in the present case we do not expect strong changes when taking an improved (retarded) screening model for the following reasons: First, the calculations are performed for 85-fs pulses and thus the density is still very low at these very early times. Second, and more important, the increase in the matrix element due to a reduced screening occurs mainly at small wave vectors. In contrast to a dephasing rate approximation, where all scattering processes give the same contribution to the dephasing, here we have seen that scattering processes with small momentum exchange are inefficient for the dynamics of both distribution functions and polarization and therefore we do not expect a strongly enhanced dephasing.

The proposed Monte Carlo procedure can be regarded as a generalization of the more conventional EMC technique to the case of physical quantities with complex value such as the interband polarization or any other physical quantity, which reflects some phase information (e.g., Fourier components of distribution functions in the analysis of four-wave-mixing experiments[34]). This clearly shows that the Monte Carlo method in this more general formulation is not limited to incoherent dynamics of classical particles. On the contrary, it can be applied to simulate any complex (classical or quantum) variable.[31]

As generally accepted, the Monte Carlo method, based on the so-called ''importance sampling,''[32] is the most efficient approach for the analysis of incoherentlike dynamics with complicated scattering processes. This high efficiency is due to a ''natural'' distribution of statistical sampling, i.e., the computer time (proportional to the statistical sampling) spent for a given **k**-space region is always proportional to the magnitude of the physical quantity of interest in this region as well as to the scattering rates determining its time evolution. As a consequence, while the computer time required for a direct integration of a rate equation is only determined by the particular choice of the **k** space and time discretizations, the Monte Carlo solution automatically evolves according to the

natural time scale, i.e., that one given by the scattering rates,[38] and devotes computer time only to the energy regions of physical interest.

As a result, the computer time spent in a Monte Carlo simulation reflects the role played by incoherent processes, e.g., cc and cp scattering events. Therefore, the combination of direct and Monte Carlo solutions on which our approach is based constitutes a natural way of splitting coherent and incoherent dynamics: When the phenomenon under investigation is a typically coherent one, i.e., the typical time scale of the dynamics is determined by the coherent terms, most of the computer time will be devoted to the direct integration while only a negligible fraction will be spent for the Monte Carlo simulation of the rare scattering processes. On the contrary, when the dynamics is dominated by incoherent phenomena, i.e., scattering rates determine the typical time scale as in the case of energy relaxation and dephasing, most of the computer time will be devoted to the Monte Carlo simulation. From these considerations, we see that the question whether one should prefer a Monte Carlo technique or a direct integration in general is ill defined, the answer depending on the nature (mainly coherent or mainly incoherent) of the phenomenon under investigation. As discussed above, the present approach combines the advantages of both techniques by automatically splitting the computer time according to the relevance of the particular regime.

## ACKNOWLEDGMENTS

We would like to thank Stephan W. Koch for many stimulating discussions. This work has been supported by the Deutsche Forschungsgemeinschaft through the Sonderforschungsbereich 383 and by the European Commission through the Network ULTRAFAST.

## APPENDIX A

For the sake of completeness, here we summarize the formulas related to the statically screened Coulomb potential as has been used in the calculations. The matrix element is given by[26]

$$V_{\mathbf{q}}^{s}=\frac{4\pi e^{2}}{\varepsilon_{s}\mathscr{V}}\,\frac{1+\alpha q^{2}}{\kappa^{2}+q^{2}+\alpha q^{4}}, \tag{A1}$$

with

$$\alpha=\frac{\varepsilon_{s}\hbar^{2}\kappa^{2}}{16\pi m_{r}ne^{2}}, \tag{A2}$$

the screening wave vector

$$\kappa^{2}=-\frac{4\pi e^{2}}{\varepsilon_{s}\mathscr{V}}\sum_{\mathbf{k},\nu}\left(\frac{\partial\epsilon_{\mathbf{k}}^{\nu}}{\partial k}\right)^{-1}\left(\frac{\partial f_{\mathbf{k}}^{\nu}}{\partial k}\right), \tag{A3}$$

the crystal volume $\mathscr{V}$, the reduced mass $m_r$, and the static dielectric constant $\varepsilon_s$.

When using a screened Coulomb potential the exchange self-energy has to be supplemented by the Coulomb hole term.[26] The total self-energy of electrons and holes in Hartree-Fock approximation is then given by

$$\hbar\Omega_{\mathbf{k}}^{e,h(\mathrm{cc},1)}=-\sum_{\mathbf{k}'}V_{\mathbf{k}-\mathbf{k}'}^{s}f_{\mathbf{k}'}^{e,h}+\frac{1}{2}\sum_{\mathbf{k}'}[V_{\mathbf{k}'}^{s}-V_{\mathbf{k}'}]. \tag{A4}$$

## APPENDIX B

By using the Heisenberg equations of motion, the equation of motion for the two-particle correlation in Eq. (20) is given by

$$\begin{aligned}
i\hbar\frac{d}{dt}\delta\langle c_{\mathbf{k}}^{\dagger}c_{\mathbf{k}'}^{\dagger}c_{\mathbf{k}'+\mathbf{q}}c_{\mathbf{k}-\mathbf{q}}\rangle=&(-\epsilon_{\mathbf{k}}^{e}-\epsilon_{\mathbf{k}'}^{e}+\epsilon_{\mathbf{k}'+\mathbf{q}}^{e}+\epsilon_{\mathbf{k}-\mathbf{q}}^{e})\,\delta\langle c_{\mathbf{k}}^{\dagger}c_{\mathbf{k}'}^{\dagger}c_{\mathbf{k}'+\mathbf{q}}c_{\mathbf{k}-\mathbf{q}}\rangle+\sum_{\mathbf{k}'',\mathbf{q}'}V_{\mathbf{q}'}\{[-\langle c_{\mathbf{k}-\mathbf{q}'}^{\dagger}c_{\mathbf{k}''+\mathbf{q}'}^{\dagger}c_{\mathbf{k}''}c_{\mathbf{k}'}^{\dagger}c_{\mathbf{k}'+\mathbf{q}}c_{\mathbf{k}-\mathbf{q}}\rangle\\
&-\langle c_{\mathbf{k}}^{\dagger}c_{\mathbf{k}'-\mathbf{q}'}^{\dagger}c_{\mathbf{k}''+\mathbf{q}'}^{\dagger}c_{\mathbf{k}''}c_{\mathbf{k}'+\mathbf{q}}c_{\mathbf{k}-\mathbf{q}}\rangle+\langle c_{\mathbf{k}}^{\dagger}c_{\mathbf{k}'}^{\dagger}c_{\mathbf{k}''+\mathbf{q}'}^{\dagger}c_{\mathbf{k}''}c_{\mathbf{k}'+\mathbf{q}-\mathbf{q}'}c_{\mathbf{k}-\mathbf{q}}\rangle\\
&+\langle c_{\mathbf{k}}^{\dagger}c_{\mathbf{k}'}^{\dagger}c_{\mathbf{k}'+\mathbf{q}}c_{\mathbf{k}''+\mathbf{q}'}^{\dagger}c_{\mathbf{k}-\mathbf{q}-\mathbf{q}'}\rangle+\langle c_{\mathbf{k}-\mathbf{q}'}^{\dagger}d_{-\mathbf{k}''}^{\dagger}d_{-\mathbf{k}''-\mathbf{q}'}c_{\mathbf{k}'}^{\dagger}c_{\mathbf{k}'+\mathbf{q}}c_{\mathbf{k}-\mathbf{q}}\rangle\\
&+\langle c_{\mathbf{k}}^{\dagger}c_{\mathbf{k}'-\mathbf{q}'}^{\dagger}d_{-\mathbf{k}''}^{\dagger}d_{-\mathbf{k}''-\mathbf{q}'}c_{\mathbf{k}'+\mathbf{q}}c_{\mathbf{k}-\mathbf{q}}\rangle-\langle c_{\mathbf{k}}^{\dagger}c_{\mathbf{k}'}^{\dagger}d_{-\mathbf{k}''-\mathbf{q}'}^{\dagger}d_{-\mathbf{k}''}c_{\mathbf{k}'+\mathbf{q}-\mathbf{q}'}c_{\mathbf{k}-\mathbf{q}}\rangle\\
&-\langle c_{\mathbf{k}}^{\dagger}c_{\mathbf{k}'}^{\dagger}c_{\mathbf{k}'+\mathbf{q}}d_{-\mathbf{k}''-\mathbf{q}'}^{\dagger}d_{-\mathbf{k}''}c_{\mathbf{k}-\mathbf{q}-\mathbf{q}'}\rangle]+\delta_{\mathbf{k}',\mathbf{k}-\mathbf{q}}f_{\mathbf{k}'}^{e}[\langle c_{\mathbf{k}}^{\dagger}c_{\mathbf{k}''}^{\dagger}c_{\mathbf{k}''+\mathbf{q}'}c_{\mathbf{k}-\mathbf{q}'}\rangle-\langle c_{\mathbf{k}-\mathbf{q}'}^{\dagger}c_{\mathbf{k}''+\mathbf{q}'}^{\dagger}c_{\mathbf{k}''}c_{\mathbf{k}}\rangle\\
&-\langle c_{\mathbf{k}}^{\dagger}d_{-\mathbf{k}''-\mathbf{q}'}^{\dagger}d_{-\mathbf{k}''}c_{\mathbf{k}-\mathbf{q}'}\rangle+\langle c_{\mathbf{k}-\mathbf{q}'}^{\dagger}d_{-\mathbf{k}''}^{\dagger}d_{-\mathbf{k}''-\mathbf{q}'}c_{\mathbf{k}}\rangle]+\delta_{\mathbf{k}',\mathbf{k}-\mathbf{q}}f_{\mathbf{k}}^{e}[\langle c_{\mathbf{k}'}^{\dagger}c_{\mathbf{k}''}^{\dagger}c_{\mathbf{k}''+\mathbf{q}'}c_{\mathbf{k}'-\mathbf{q}'}\rangle\\
&-\langle c_{\mathbf{k}'-\mathbf{q}'}^{\dagger}c_{\mathbf{k}''+\mathbf{q}'}^{\dagger}c_{\mathbf{k}''}c_{\mathbf{k}'}\rangle-\langle c_{\mathbf{k}'}^{\dagger}d_{-\mathbf{k}''-\mathbf{q}'}^{\dagger}d_{-\mathbf{k}''}c_{\mathbf{k}'-\mathbf{q}'}\rangle+\langle c_{\mathbf{k}'-\mathbf{q}'}^{\dagger}d_{-\mathbf{k}''}^{\dagger}d_{-\mathbf{k}''-\mathbf{q}'}c_{\mathbf{k}'}\rangle]\}.
\end{aligned} \tag{B1}$$

In order to truncate the hierarchy of equations on this level, the expectation values of six operators (three-particle density matrices) have to be factorized into distribution functions and polarizations. Renormalization and correlation effects can be taken into account if additional contributions obtained by a factorization into single-particle density matrices and two-particle correlations are included. Here, however, we will neglect these terms. Correlation effects are partially taken into account by using the screened Coulomb potential. Energy renormalizations are of minor importance since typically the dominant term is a rigid shift of the bands, which cancels in the energy differences relevant for intraband scattering processes. With these approximations, the first term reads

$$\langle c_{\mathbf{k}-\mathbf{q}'}^{\dagger}c_{\mathbf{k}''+\mathbf{q}'}^{\dagger}c_{\mathbf{k}''}c_{\mathbf{k}'}^{\dagger}c_{\mathbf{k}'+\mathbf{q}}c_{\mathbf{k}-\mathbf{q}}\rangle=f_{\mathbf{k}-\mathbf{q}'}^{e}f_{\mathbf{k}}^{e}f_{\mathbf{k}'}^{e}\delta_{\mathbf{k}'',\mathbf{k}-\mathbf{q}'}\delta_{\mathbf{k}',\mathbf{k}-\mathbf{q}}+f_{\mathbf{k}-\mathbf{q}}^{e}f_{\mathbf{k}'+\mathbf{q}}^{e}(1-f_{\mathbf{k}'}^{e})\,\delta_{\mathbf{k}'',\mathbf{k}'}(\delta_{\mathbf{q}',\mathbf{q}}-\delta_{\mathbf{q}',\mathbf{k}-\mathbf{k}'-\mathbf{q}}). \tag{B2}$$

Collecting all contributions, the equation of motion is then given by

$$i\hbar\frac{d}{dt}\delta\langle c_{\mathbf{k}}^{\dagger}c_{\mathbf{k}'}^{\dagger}c_{\mathbf{k}'+\mathbf{q}}c_{\mathbf{k}-\mathbf{q}}\rangle=(-\epsilon_{\mathbf{k}}^{e}-\epsilon_{\mathbf{k}'}^{e}+\epsilon_{\mathbf{k}'+\mathbf{q}}^{e}+\epsilon_{\mathbf{k}-\mathbf{q}}^{e})\,\delta\langle c_{\mathbf{k}}^{\dagger}c_{\mathbf{k}'}^{\dagger}c_{\mathbf{k}'+\mathbf{q}}c_{\mathbf{k}-\mathbf{q}}\rangle+(V_{\mathbf{q}}-V_{\mathbf{k}-\mathbf{k}'-\mathbf{q}})[f_{\mathbf{k}}^{e}f_{\mathbf{k}'}^{e}(1-f_{\mathbf{k}'+\mathbf{q}}^{e})(1-f_{\mathbf{k}-\mathbf{q}}^{e})$$
$$-f_{\mathbf{k}-\mathbf{q}}^{e}f_{\mathbf{k}'+\mathbf{q}}^{e}(1-f_{\mathbf{k}'}^{e})(1-f_{\mathbf{k}}^{e})]+V_{\mathbf{q}}[p_{\mathbf{k}-\mathbf{q}}p_{\mathbf{k}}^{*}(f_{\mathbf{k}'+\mathbf{q}}^{e}-f_{\mathbf{k}'}^{e})+p_{\mathbf{k}'+\mathbf{q}}p_{\mathbf{k}'}^{*}(f_{\mathbf{k}-\mathbf{q}}^{e}-f_{\mathbf{k}}^{e})]$$
$$-V_{\mathbf{k}-\mathbf{k}'-\mathbf{q}}[p_{\mathbf{k}-\mathbf{q}}p_{\mathbf{k}'}^{*}(f_{\mathbf{k}'+\mathbf{q}}^{e}-f_{\mathbf{k}}^{e})+p_{\mathbf{k}'+\mathbf{q}}p_{\mathbf{k}}^{*}(f_{\mathbf{k}-\mathbf{q}}^{e}-f_{\mathbf{k}'}^{e})]. \tag{B3}$$

Formally integrating Eq. (B3) and performing a Markov approximation as in the case of cp interaction results in the second-order contributions given by Eqs. (21)–(26). In these equations exchange contributions, i.e., terms proportional to $V_{\mathbf{q}}V_{\mathbf{k}-\mathbf{k}'-\mathbf{q}}$, have been neglected with respect to the direct terms proportional to $|V_{\mathbf{q}}|^2$, which, except for very high densities, is usually a good approximation due to the strongly peaked shape of the matrix element.

*Present address: Institut für Theoretische Physik II, Westfälische Wilhelms-Universität, Wilhelm-Klemm-Strasse 10, 48149 Münster, Germany; Fax: +49251833669. Electronic address: kuhnti@nwz.uni-muenster.de

[1] C. Jacoboni and L. Reggiani, Rev. Mod. Phys. **55**, 645 (1983).
[2] L. Reggiani, *Hot Electron Transport in Semiconductors* (Springer, Berlin, 1985).
[3] P. Lugli *et al.*, Phys. Rev. B **39**, 7852 (1989).
[4] S. M. Goodnick and P. Lugli, in *Hot Carriers in Semiconductor Nanostructures: Physics and Applications*, edited by J. Shah (Academic, San Diego, 1992), p. 191.
[5] L. Rota, P. Lugli, T. Elsaesser, and J. Shah, Phys. Rev. B **47**, 4226 (1993).
[6] M. A. Osman and D. K. Ferry, Phys. Rev. B **36**, 6018 (1987).
[7] M. Rieger *et al.*, Solid State Electron. **31**, 687 (1988).
[8] D. W. Bailey, C. J. Stanton, and K. Hess, Phys. Rev. B **42**, 3423 (1990).
[9] K. El Sayed, T. Wicht, H. Haug, and L. Bányai, Z. Phys. B **86**, 345 (1992).
[10] M. V. Fischetti and S. E. Laux, Phys. Rev. B **38**, 9721 (1988).
[11] S. E. Laux, M. V. Fischetti, and D. J. Frank, IBM J. Res. Dev. **34**, 466 (1990).
[12] C. Jacoboni and P. Lugli, *The Monte Carlo Method for Semiconductor Device Simulations* (Springer, Wien, 1989).
[13] J. Shah, Solid State Electron. **32**, 1051 (1989).
[14] H. Kurz, Semicond. Sci. Technol. **7**, B124 (1992).
[15] U. Hohenester *et al.*, Phys. Rev. B **47**, 13 233 (1993).
[16] A. Leitenstorfer *et al.*, Phys. Rev. Lett. **73**, 1687 (1994).
[17] A. Alexandrou, V. Berger, and D. Hulin, Phys. Rev. B **52**, 4654 (1995).
[18] F. Rossi, S. Haas, and T. Kuhn, Phys. Rev. Lett. **72**, 152 (1994).
[19] T. Kuhn, S. Haas, and F. Rossi, Phys. Status Solidi B **188**, 417 (1995).
[20] S. Schmitt-Rink, D. S. Chemla, and H. Haug, Phys. Rev. B **37**, 941 (1988).
[21] M. Lindberg and S. W. Koch, Phys. Rev. B **38**, 3342 (1988).
[22] R. Binder *et al.*, Phys. Rev. B **45**, 1107 (1992).
[23] T. Kuhn and F. Rossi, Phys. Rev. B **46**, 7496 (1992).
[24] T. Kuhn and F. Rossi, Phys. Rev. Lett. **69**, 977 (1992).
[25] T. Elsaesser, J. Shah, L. Rota, and P. Lugli, Phys. Rev. Lett. **66**, 1757 (1991).
[26] H. Haug and S. W. Koch, *Quantum Theory of the Optical and Electronic Properties of Semiconductors* (World Scientific, Singapore, 1993).
[27] D. K. Ferry, *Semiconductors* (Macmillan, New York, 1991).
[28] J. Schilp, T. Kuhn, and G. Mahler, Phys. Rev. B **50**, 5435 (1994).
[29] V. M. Axt and A. Stahl, Z. Phys. B **93**, 195 (1994).
[30] G. F. Kuras and P. Kocevar (unpublished). It turns out that the main effect of these terms is to somewhat increase the density, i.e., to increase the Coulomb enhancement. The shape of the distribution functions is essentially unaffected.
[31] F. Rossi, P. Poli, and C. Jacoboni, Semicond. Sci. Technol. **7**, 1017 (1992).
[32] M. H. Kalos and K. A. Whitlock, *Monte Carlo Methods Vol. 1: Basics* (Wiley, New York, 1986).
[33] A. Lohner *et al.*, Phys. Rev. Lett. **71**, 77 (1993).
[34] A. Leitenstorfer *et al.*, Phys. Rev. B **49**, 16 372 (1994).
[35] J. A. Kash, Phys. Rev. B **40**, 3455 (1989).
[36] G. Fasol *et al.*, Phys. Rev. B **41**, 1461 (1990).
[37] Due to its definition, $|R_{\mathbf{k}}|$ exhibits an increased numerical noise in regions where $p_{\mathbf{k}}$ is very small [see, e.g., Fig. 9(c)]. Furthermore, $\Delta\varphi_{\mathbf{k}}$ is numerically not well defined and strongly fluctuates if $|R_{\mathbf{k}}|$ is very small [see, e.g., Figs. 7(a) and 8(a)]. However, this numerical noise is irrelevant for the evolution of the physical quantity $p_{\mathbf{k}}$ and it is again an example of the fact that in a Monte Carlo simulation the accuracy is mainly devoted to those regions in **k** space that are important for the dynamics.
[38] However, it should be noted that the self-scattering technique commonly used in the Monte Carlo simulation (Ref. 12) leads in some particular cases to strong overestimations of the scattering rates and, therefore, to typical simulation time scales shorter than the corresponding physical ones.